Chemical Engineering Journal xxx (2011) xxx–xxx

Contents lists available at ScienceDirect

Chemical Engineering Journal

journal homepage: www.elsevier.com/locate/cej

Simulations of gravity-driven flow of binary liquids in microchannels

A. Kuzmin [a,*], M. Januszewski [b], D. Eskin [c], F. Mostowfi [c], J.J. Derksen [a]

[a] Chemical and Materials Engineering, University of Alberta, 7th Floor, ECERF, 9107 116 St, Edmonton, Alberta, T6G 2V4, Canada
[b] Insitute of Physics, University of Silesia, 40-007 Katowice, Poland
[c] DBR Schlumberger Technology Center, 9450 17 Ave NW, Edmonton, Alberta, T6N 1M9, Canada

ARTICLE INFO

Article history:
Received 7 January 2011
Received in revised form 11 April 2011
Accepted 14 April 2011

Keywords:
Bretherton problem
Microchannel simulation
Multiphase flow
Lattice Boltzmann method
Binary liquid model
Flow between plates
Gravity driven

ABSTRACT

In this work a free-energy binary liquid lattice-Boltzmann scheme is used to simulate Taylor/Bretherton flow in a micro-channel where elongated gas bubbles move through a liquid with thin liquid films between the bubbles and the channel walls. The numerical scheme has a diffuse interface, and a main focus of our work is to assess resolution requirements for correctly resolving the liquid film and bubble motion. The simulations are two-dimensional and span a capillary number range of 0.05–1.0 where the capillary number is based on the liquid dynamic viscosity, the velocity of the bubble, and the interfacial tension. The flow is driven by a body force, and periodic boundary conditions apply in the streamwise direction. We obtain grid independent results as long as the liquid film thickness is at least twice the width of the diffuse interface, with film thicknesses in accordance to literature results. We also show that the results in terms of film thicknesses are largely insensitive to the liquid–gas viscosity ratio and wettability parameters.

1. Introduction

The Taylor/Bretherton [1] flow deals with long gas bubbles moving through liquid in narrow channels, Fig. 1. It was found that the front meniscus film thickness is proportional to $Ca^{2/3}$ for capillary numbers smaller than 0.003, where the capillary number is defined as:

$$Ca = \frac{\mu_{liq} U_{bubble}}{\gamma}, \quad (1)$$

where μ_{liq} is the liquid viscosity, U_{bubble} is the bubble velocity, and γ is the interfacial tension between gas and liquid.

While there are many works which simulate the Bretherton problem by the boundary value approach [2,3], those methods are of limited applicability for problems involving complex geometries, free interface motion, or coalescence and/or droplet breakup. The continuous interface models are more flexible for those kinds of simulations. However, if the interface is smeared out over several grid nodes, the question of proper film resolution in comparison with the interface resolution arises. This work is focused on exploring the parameter range of the binary liquid lattice Boltzmann method to resolve correctly the flow in a range of capillary numbers.

The lattice Boltzmann method (LBM) has emerged as a successful method to simulate a wide variety of phenomena including hydrodynamics [4], thermal flows [5], microflows [6], ferrofluids [7], and multiphase flows [8,9]. Thanks to its kinetic nature, LBM as a particle method easily tackles complex geometries and allows incorporation of physical phenomena on the microscopic level, as in the case of multiphase models. Most multiphase lattice Boltzmann models [8,9] resolve the interface using continuous interface methods where the interface spans over several grid nodes. Such a representation brings issues of the film thickness resolution versus interface resolution – the diffuse interface should be dealt with in such a way as to have a negligible effect on the physics of the film.

The binary liquid free-energy LB model due to Swift et al. [8] we used simulates two liquids with the assumption of uniform overall density. While the classical Bretherton problem is stated for gas and liquid, which are of significantly different densities and viscosities, it was indicated [1] that inertia effects were negligible. Moreover, the results of Giavedoni and Saita [10] and Heil [3] show insignificant Reynolds number (Re) effects on the film thickness for a relatively wide range of Reynolds numbers. For example, Giavedoni and Saita [10] suggested that the Reynolds number effects are negligible for $Ca \leq 0.05$ and have moderate impact for $Ca > 0.05$ in the range of Reynolds number from 0 to 70. Later on, Heil [3] extended these results up to $Re = 300$. They indicate that while the Reynolds number influence on the established film thickness is insignificant (7 percent from the film thickness measured at $Re = 0$), the pressure distribution and the flow field near the front bubble tip can be affected by changes in Re. Since in the present work we

* Corresponding author. Tel.: +1 780 729 3695.
E-mail addresses: kuzmin@ualberta.ca (A. Kuzmin), michalj@gmail.com (M. Januszewski), deskin@slb.com (D. Eskin), fmostowfi@slb.com (F. Mostowfi), jos@ualberta.ca (J.J. Derksen).

1385-8947/$ – see front matter © 2011 Elsevier B.V. All rights reserved.
doi:10.1016/j.cej.2011.04.023

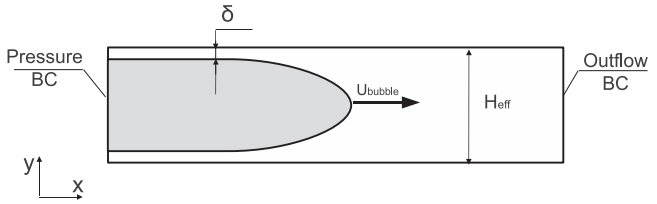

Fig. 1. The classical Bretherton problem layout. The gas bubble propagates with the steady velocity U_{bubble} through the liquid media and deposits the film, where the thickness to height of the channel H_{eff} ratio is δ.

only deal with flows with Re < 20, we can safely neglect any inertia effects and conclude that the major governing parameter for microchannel Bretherton flows is not the density ratio, but the viscosity ratio. Moreover, the results based on uniform density, as in the case of the LBM binary liquid model, are in good agreement with other simulations [10,3] in which inertia effects were taken into account.

Resolving the interface on a fine level for capillary numbers smaller than 0.003 is computationally expensive even in the two-dimensional case (the amount of memory necessary to perform the simulation would be of the order of tens or hundreds of gigabytes). This work is therefore based on a comparison of the results obtained with the known data validated for the Bretherton bubble flow. In this paper, we present techniques for initialization of the simulations and discuss optimal parameter ranges for the binary liquid LB model, such as the binary liquid parameters, the viscosity ratio and the grid resolution. The emphasis is to obtain correct flow physics, especially in terms of film thicknesses.

The paper is organized as follows. First, we review the literature for the Bretherton problem and briefly explain the binary liquid lattice Boltzmann model. Then, the parameters involved in the simulation are examined and presented in the results section. The paper is concluded with a summary of the main findings.

2. Bretherton bubble flow

Bretherton [1] studied a long bubble moving in a tube filled with liquid. It was found that the film thickness is proportional to $Ca^{2/3}$ in the range of small capillary numbers. Later, it was realized [11,12] that the film thickness is proportional to $Ca^{2/3}$ only in the certain region behind the front meniscus and that the film thickness varies over the bubble length for bubbles of finite length. Numerical simulations [10] and experimental studies [13] showed a deviation from the $Ca^{2/3}$ rule for capillary numbers larger than 0.003. To consistently predict a flow pattern for capillaries in different ranges of parameters, simulations have been conducted and have been typically validated with the small capillary numbers Bretherton problem.

There are a number of numerical methods which were used for the simulation of the Taylor/Bretherton flow. van Baten and Krishna [14] studied the mass transfer and film thickness for rising bubbles in a circular capillary using the finite volume method. Kreutzer et al. [13] also used the finite volume method to perform simulations of a circular capillary for a number of different Reynolds and capillary numbers. Wong et al. [11,12] studied three-dimensional bubbles in polygonal capillaries and calculated bubble shapes in the slug cross sections and menisci appearance. Heil [3] and Ingham and Ritchie [2] studied gas finger propagation in a two-dimensional channel for a range of Reynolds and capillary numbers using the finite element method. Giavedoni and Saita [10] performed cross validation of the finite element solution with previously published results. The solutions were obtained for circular and planar geometries.

While the applicability of other methods has been demonstrated for the simulation of the Bretherton/Taylor problem, this is not the case for the lattice Boltzmann method. A thorough parametric study for this approach has not been done to the best of the authors' knowledge.

One should acknowledge the work of Ledesma-Aguilar et al. [15] on menisci in thin films for fingering phenomena, as well as the work of Yang et al. [16] who performed lattice Boltzmann simulations of two-dimensional channel flows for relatively large capillary numbers, and found discrepancies with the classical Bretherton theory, which is limited to the low capillary number regime [10]. These authors did not take into account recent studies extending microchannel simulations for the capillary numbers beyond the Bretherton regime. Thus, the comparison with other established CFD methods is limited. Yang et al. used the Shan–Chen model [9] to simulate the multiphase behavior. The Shan–Chen model is also a continuous interface model, but the above-mentioned paper does not contain a study of grid dependence.

The level set method is also represented by a number of works [17–19]. While the bubble shapes were found to be in a good agreement with the experiments, the range of studied bubble lengths is limited to 2–3 channel diameters. Thus, the bubble radius changes significantly and cannot be used as a classical Bretherton problem benchmark. However, the works provide insight to the bubble formation and to the way small bubbles flow in microchannels.

3. Lattice Boltzmann binary liquid model

The lattice Boltzmann equation (LBE) operates on a rectangular grid representing the physical domain. It utilizes probability distribution functions (also known as particle populations) containing information about macroscopic variables, such as fluid density and momentum. LBE consists of two parts: a local collision step, and a propagation step which transports information from one node to another along some directions specified by the discrete velocity set. The LBE is typically implemented as follows:

$$\begin{aligned} f_i^*(\boldsymbol{x}, t) &= \omega f_i^{eq}(\boldsymbol{x}, t) - (1-\omega) f_i(\boldsymbol{x}, t) + F_i, \quad \text{collision step} \\ f_i(\boldsymbol{x} + \boldsymbol{c_i}, t+1) &= f_i^*(\boldsymbol{x}, t), \qquad\qquad\qquad\quad \text{propagation step,} \end{aligned} \tag{2}$$

where f_i is the probability distribution function in the direction $\boldsymbol{c_i}$, f_i^{eq} is the equilibrium probability distribution function, ω is the relaxation parameter, and F_i is the external force population. The force population represents an external physical force and is implemented in the current work using the scheme outlined in Guo et al. [20].

The binary fluid LB model is based on a free-energy functional [8,21], and operates with two sets of populations: one to track the pressure and the velocity fields, and another to represent the phase field ϕ indicating the gas or liquid.

The model we use is a two-dimensional nine-velocity (D2Q9) model, with equilibrium populations [22]:

$$\begin{aligned} f_i^{eq} &= w_i \left(3p_0 - k\phi\Delta\phi + \rho \frac{u_\alpha c_{i\alpha}}{c_s^2} + \rho \frac{Q_{i\alpha\beta} u_\alpha u_\beta}{2c_s^4} \right) \\ &\quad + k(w_i^{xx}(\partial_x\phi)^2 + w_i^{yy}(\partial_y\phi)^2 + w_i^{xy}\partial_x\phi\partial_y\phi), \quad 1 \le i \le 8 \\ f_0^{eq} &= \rho - \sum_{i \neq 0} f_i^{eq} \\ g_i^{eq} &= w_i \left(\Gamma\mu + \phi \frac{c_{i\alpha} u_{i\alpha}}{c_s^2} + \phi \frac{Q_{i\alpha\beta} u_\alpha u_\beta}{2c_s^4} \right), \quad 1 \le i \le 8 \\ g_0^{eq} &= \phi - \sum_{i \neq 0} g_i^{eq}, \end{aligned} \tag{3}$$

where Γ is the mobility parameter; the chemical potential $\mu = -A\phi + A\phi^3 - k\Delta\phi$; k is the parameter related to the surface

tension; A is the parameter of the free-energy model. The bulk pressure is expressed as $p_0 = c_s^2\rho + A(-0.5\phi^2 + 0.75\phi^4)$ with the sound speed $c_s^2 = 1/3$. Parameters specific to the D2Q9 grid are the weights $w_i = \{4/9, 1/9, 1/9, 1/9, 1/9, 1/36, 1/36, 1/36, 1/36\}$, and the tensor $Q_{i\alpha\beta} = c_{i\alpha}c_{i\beta} - c_s^2\delta_{\alpha\beta}$. Other weights are as follows: $w_{1-2}^{xx} = w_{3-4}^{yy} = 1/3$, $w_{3-4}^{xx} = w_{1-2}^{yy} = -1/6$, $w_{5-8}^{xx} = w_{5-8}^{yy} = -1/24$, $w_{1-4}^{xy} = 0$, $w_{5-6}^{xy} = 1/4$ and $w_{7-8}^{xy} = -1/4$. The set of equations (3) restores the macroscopic fluid equations as:

$$\begin{aligned} &\partial_t\rho + \partial_\alpha\rho u_\alpha = 0 \\ &\rho\left(\partial_t + u_\beta\partial_\beta\right)u_\alpha = F_\alpha - \partial_\beta P_{\alpha\beta} + \nu\partial_\beta\left(\partial_\alpha u_\beta + \partial_\beta u_\alpha\right) \\ &\partial_t\phi + \partial_\alpha\phi u_\alpha = M\partial_{\beta\beta}^2\mu, \end{aligned} \tag{4}$$

where $\nu = c_s^2(\tau - 1/2)$ is the viscosity, $M = \Gamma(\tau_\phi - 1/2)$ is the mobility parameter, and $\tau = 1/\omega$ and τ_ϕ are the relaxation parameters of density and phase fields, $P_{\alpha\beta} = (p_0 - k\phi\Delta\phi - k/2\,|\nabla\phi|^2)\delta_{\alpha\beta} + k\partial_\alpha\phi\partial_\beta\phi$ [22]. The interface tension value in the framework of the binary liquid model is $\gamma = \sqrt{8kA/9}$. The inclusion of the interface tension in the momentum flux tensor is done through the coefficients k, A and weights $w_i^{\alpha\beta}$.

Note that the first equation of system (2) simulates the continuity and the Navier–Stokes equations, i.e. the first two equations in (4). The second equation of system (2) simulates the phase governing equation, i.e. the third equation in (4). The system (4) allows the separation of the liquid phase with $\phi = 1$ and a so-called gas phase with $\phi = -1$. The relaxation time is taken as linearly dependent on the relaxation times τ_{gas} and τ_{liq}: $\tau = \tau_{gas} + ((\phi + 1)/2)(\tau_{liq} - \tau_{gas})$. This allows to change viscosity from the gas viscosity $\nu_{gas} = 1/3(\tau_{gas} - 1/2)$ to the liquid viscosity $\nu_{liq} = 1/3(\tau_{liq} - 1/2)$ while phase changes accordingly.

While the lattice Boltzmann system has parameters such as the surface tension, the gas and liquid viscosities, etc., those parameters are not the representative and proportional quantities of the parameters in a physical system. The parameters of the lattice Boltzmann are connected with the physical parameters only through the non-dimensional numbers governing the physics of the problem. In our case, these numbers are the capillary number Ca and the viscosity ratio μ_{liq}/μ_{gas}, which are obtained from the physical world and then matched through the lattice Boltzmann quantities. The set of the fluid and phase equations (4) is valid in the lattice Boltzmann space and in the physical domain. Therefore, one can substitute any quantity, i.e. U_{bubble}, in the physical units or in the lattice Boltzmann units as soon as the capillary number is the same in both worlds.

4. Numerical benchmark procedure

To properly simulate and compare simulation results with the data published in the literature, one needs to design a numerical benchmark addressing the following challenges for the lattice Boltzmann method:

- The diffuse nature of the interface in the multiphase model should not influence the film thickness results. The same applies to spurious currents arising due to surface tension discretization, which can influence mass transfer in the thin film, thereby compromising the overall solution.
- The wettability coefficient which in principle can control the dynamic angle and the menisci appearance [23] should not influence the overall solution.
- The free-energy model examined in this work is a single density, two viscosities model. The classical Bretherton problem is a free-interface problem between liquid and gas where the film thickness is established by itself. Thus, the viscosity and the density ratios for the classical Bretherton problem should be large. However, in terms of the lattice Boltzmann binary liquid framework only the viscosity ratio can be addressed. Our computations show that the results are consistent with other works and inertial effects can be neglected.
- The Bretherton problem addresses a bubble flow driven by a pressure difference, not a body force. However, to the best of our knowledge the pressure boundary conditions are still not yet developed for the binary liquid model, because it involves the treatment of associated gradients and Laplacians on the boundary. This kind of pressure boundary conditions for the binary liquid model is currently under development, and preliminary results show that the differences between flows driven by a body force and by pressure difference are small as far as the film thickness is concerned. In this work we limit ourselves to the study of body force driven flows, because of their simplicity and better numerical stability. This implies that we can use periodic boundary conditions in the streamwise direction. As soon as the periodic boundary conditions are applied, not a single bubble but a bubble train is simulated. In this case one needs to ensure that the distance between bubbles is large enough to exclude mutual bubble influence.
- Most simulations are done for a channel with circular cross section, which is quite difficult to address in terms of lattice Boltzmann framework. Although one can apply certain finite difference stencils [24,25] developed specifically for curved boundaries, the analysis of error introduced by the boundary conditions becomes an issue. Although the circular axis-symmetric case can be simulated on a rectangular grid by introducing specific mass and force terms in the continuity and Navier–Stokes equation [26], the lattice Boltzmann incorporation of force and mass terms is in the process of development and validation. Therefore, the benchmark is chosen as a plane-symmetric two-dimensional case.

Given all the concerns and challenges, the suggested lattice Boltzmann framework is a two-dimensional flow driven by a body force. An analytical solution to this problem is not known for a wide range of capillary numbers. Though some authors [16] use the gravity driven model to validate the Bretherton film thickness, the latter should be used with caution since the velocity of the bubble is different from the fluid velocity and the bubble shape is different in the front and rear menisci depending on the Bond number ($Bo = \Delta\rho g l^2/\gamma$). Wong et al. [11] analytically described the film thickness variation along a bubble varying from $Ca^{1/2}$ to $Ca^{2/3}$. The bubble should be long enough to have the film thickness proportional to $Ca^{2/3}$. Therefore, we chose the bubble length to be 5 channel heights. This number is shown to be sufficient to give results consistent with the theory. The channel length is taken to be 3 bubble lengths (or 15 channel heights) to minimize influence of one bubble on another, because of the periodicity of boundary conditions. Fig. 2 is a sketch of the geometry used for the benchmark.

5. Results

5.1. The nondimensionalization and initialization procedure

We now introduce the procedure of nondimensionalization, as well as the initialization technique we used to determine the parameters necessary for the simulation. The capillary number defined in Eq. (1) governs the interface thickness. Parameters as μ_{liq}, γ are usually taken in the already defined stable range. The capillary number Ca is supplied from the physical world. In com-

Please cite this article in press as: A. Kuzmin, et al., Simulations of gravity-driven flow of binary liquids in microchannels, Chem. Eng. J. (2011), doi:10.1016/j.cej.2011.04.023

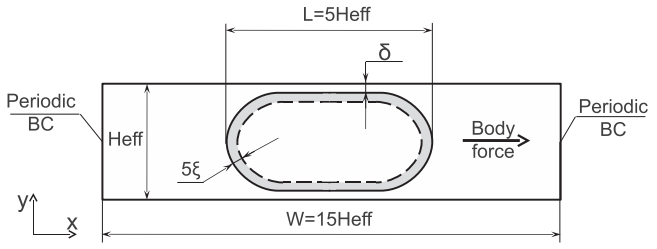

Fig. 2. The benchmark sketch. δ corresponds to film thickness. ξ corresponds to the interface thickness. We take the microchannel length to be 15 times larger than its height.

parison, the bubble velocity U_{bubble} is not given explicitly. In our simulations we approximate U_{bubble} with the Poiseuille profile maximum velocity, which is given as:

$$U_{\text{bubble}} \approx \frac{H_{\text{eff}}^2}{8\mu_{\text{liq}}}\frac{dP}{dx}$$
$$U_{\text{bubble}} \approx \frac{(N_y-2)^2}{\frac{8}{6}(\tau_{\text{liq}}-\frac{1}{2})}\frac{dP}{dx}, \quad (5)$$

where N_y is the number of nodes in the vertical direction. As will be discussed further, the effective channel width is defined as $H_{\text{eff}} = N_y - 2$ due to the use of bounce-back nodes to mimic no-slip conditions at the walls. For the Poiseuille profile one can estimate the body force (pressure gradient) through the capillary number and grid resolution:

$$\frac{dP}{dx} = \frac{8}{(N_y-2)^2}\gamma \text{Ca}. \quad (6)$$

In the simulations the body force (6) causes the bubble velocity to differ from that implied by the Poiseuille relation because of the presence of a bubble in the flow. That is why an iterative procedure is needed to achieve the desired velocity and capillary number. However, the initial body force as given by (6) is a good starting point.

After one calculates the parameters to run a simulation, one has to initialize the macroscopic fields and particle populations. The velocity is initialized with zero everywhere. Populations are initialized using the equilibrium values for the binary liquid model, including all the phase gradients and Laplacians. The liquid phase is initialized with $\phi = 1$ and the gas phase with $\phi = -1$. Though the initial film thickness does not affect the final result for the front meniscus (see Fig. 3) we keep the initialized film thickness as close as possible to the already obtained numerical film thickness values [10]. This is done to minimize the time to convergence.

For demonstration purposes we present the simulation parameters choice for Ca = 0.05. In these examples we use $k = 0.04$ and $A = 0.04$ as numerically optimal binary liquid model parameters. That implies the surface tension to be $\sqrt{8kA/9} = 0.0377$ and the characteristic width of the interface $5\sqrt{k/A} = 5$ lattice Boltzmann units (grid spacings). For the sake of simplicity and stability, the relaxation times for liquid and gas phases are taken as $\tau_{\text{liq}} = 2.5$ and $\tau_{\text{gas}} = 0.7$, which correspond to the liquid over gas kinematic viscosity ratio equal to 10.

Overall, the setting up the simulations can be described in steps as follows:

Capillary number One first needs to set the capillary number for simulations. For the demonstration purposes we chose Ca = 0.05.
Film thickness After the capillary number is prescribed, one needs to approximate the film thickness δ. It can be done either by taking correlations from numerical simulations by Heil [3] and Giavedoni and Saita [10] or by using the classical Bretherton correlation for small cappillary numbers $\delta = 0.6687\text{Ca}^{2/3}$. In the case of Ca = 0.05, the film thickness is taken from correlations by Heil [3], and for Reynolds number 40 is in the range 0.06–0.07.
Grid choice After specifying the film thickness, one needs to choose the associate number of nodes to resolve the film thickness. Note that for paremeters indicated above the interface is spread over approximately 5 lattice units. The study of the interface resolution to the film thickness, Section 5.3, suggests to choose the film thickness to be 2–2.5 times larger than the interface thickness. Therefore, we want to resolve 6% of the whole channel width with 12 lattice units. Thus, the physical channel width is 200 lattice units. We take the bubble length equal to 5 channel widths for the film thickness to establish and the distance between bubbles as 3 bubble lengths to avoid mutual influence of bubbles on each other. Thus, the whole physical grid size is 200×3000. Note that in the case of the half-way bounce-back walls [4] which are used in the simulations one needs to calculate the film thickness as:

$$\delta = \frac{\phi_0 - 0.5}{N_y - 2}, \quad (7)$$

where ϕ_0 is the grid coordinate where the phase field is 0, $N_y - 2$ is the effective channel height. If the grid size in the y direction is N_y, then one has $N_y - 1$ regions between the grid nodes which represent the physical domain. The effective wall location is in the middle between bounce-back and fluid nodes giving overall $N_y - 2$ nodes representing the fluid. Note that it is a simplification to impose the boundary in the middle between the bounce-back node and the fluid node. The location of the wall is viscosity dependent [27]. The effective location of the wall for the multiphase models to the best of the authors' knowledge is not yet derived. Thus, the simulation grid size is 202×3000.
Velocity The relaxation parameters are taken to be in the stable range for the simulations. In the present simulations the viscosity ratio is $\mu_{\text{liq}}/\mu_{\text{gas}} = 10$ with the correspoding relaxation times $\tau_{\text{liq}} = 2.5$ and $\tau_{\text{gas}} = 0.7$. Given the viscosity of the liquid one can obtain the velocity of the bubble from the capillary number:

$$U_{\text{bubble}} = \text{Ca}\frac{\gamma}{\mu_{\text{liq}}} = \text{Ca}\frac{\sqrt{8kA/9}}{1/3(\tau_{\text{liq}}-1/2)}$$
$$U_{\text{bubble}} = 0.05\frac{0.0377}{0.6666} = 2.82\times 10^{-3}, \quad (8)$$

where $\mu_{\text{liq}} = \frac{1}{3}(2.5 - 0.5) = 0.6666$.
Body force It is desired to obtain the prescribed velocity U_{bubble} in the simulations. The flow in the simulations is conducted by imposing the body force. Thus, the assumption is needed of how the body force is connected with the bubble velocity U_{bubble}. We assume that the flow is close to planar Poiseuille flow with U_{bubble} being the maximun in the Poiseuille profile:

$$\frac{dP}{dx} = \frac{8\mu_{\text{liq}}}{H_{\text{eff}}^2}U_{\text{bubble}} = \frac{8}{N_y^2}\gamma\text{Ca} = 3.77\times 10^{-7}. \quad (9)$$

After imposing the body force the simulations can be run. A typical simulation runs approximately 100,000–300,000 time steps to reach steady-state, see Section 5.2.

Note that following the prescribed procedure one can see that computer memory requirements are high for small capillary numbers due to large grids to resolve the film thickness. Thus, the simulations in the present work cover a range of capillary numbers from 0.05 to 1.0. Although, Bretherton obtained an analytical solution for the range of low capillary numbers $\text{Ca} \leq 0.005$, many researchers, for example Giavedoni and Saita [10] and Heil [3], extended it to the range of capillary numbers greater than 0.005, and to higher Reynolds numbers. Therefore, the focus of our work

Please cite this article in press as: A. Kuzmin, et al., Simulations of gravity-driven flow of binary liquids in microchannels, Chem. Eng. J. (2011), doi:10.1016/j.cej.2011.04.023

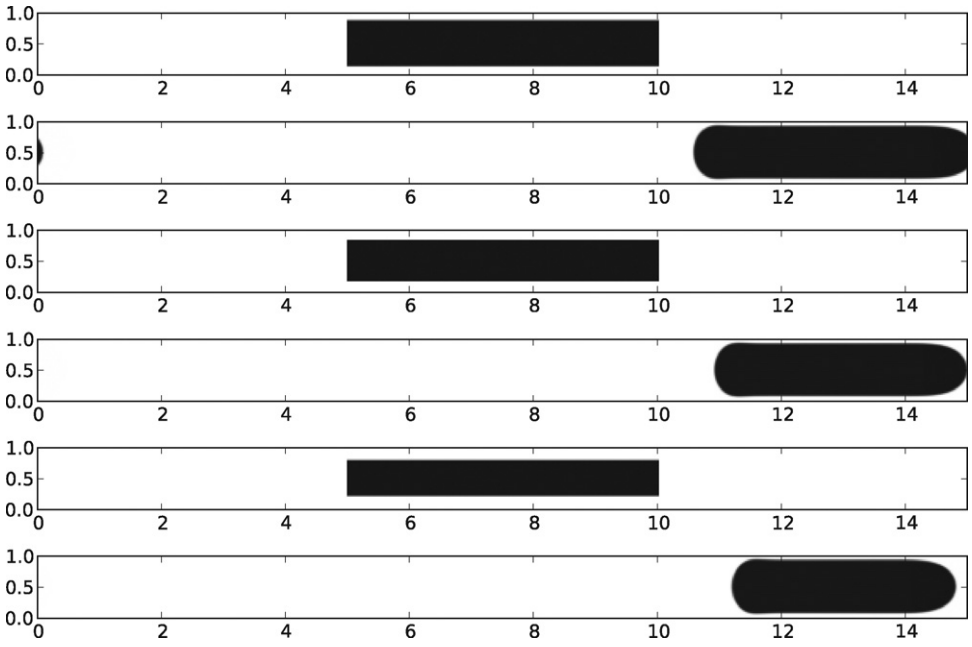

Fig. 3. Phase plots for different bubble thicknesses as $H_{\text{eff}} - 12$, $H_{\text{eff}} - 16$ and $H_{\text{eff}} - 20$. The grid for the simulation is 102×1501. The results are rescaled on N_y.The phase profiles were obtained after 2×10^5 time steps. One can see that even if the system is initialized with different bubble volumes, the bubbles always relax to a shape where the film thickness is the same. For the given parameters (Ca = 0.05) the interface thickness rescaled at the effective channel width H_{eff} is 0.0701, 0.0697, 0.0692 measured at the center of the bubble.

on the capillary range larger $\text{Ca} \geq 0.05$ is legitimate as far as we base it on comparison with already cross validated results for all ranges of capillary numbers. Our intention is to show physically correct behavior for moderate Ca, which can be easily and quickly validated on a computer.

Note that we base the initialization techniques on correlations for the capillary number and the body force. However, in the binary liquid framework those correlations are approximations. The strongest assumption is in calculating the body force from the Poiseuille velocity profile. In reality, the less viscous bubble moves faster than the surrounding liquid. In practice, one needs to take the bubble velocity from the simulations and recalculate all the necessary flow characteristics, i.e. adjust the applied force to obtain the desired velocity/capillary number. However, simulations show that the Poiseuille flow assumptions work reasonably well.

Note that the initialization procedure is a good guide of designing the simulations. For example for the grid refinement, Section 5.3, we keep the same velocity U_{bubble} and Ca. This implies the conservation of the quantity $H_{\text{eff}}^2(\text{d}P/\text{d}x) = (N_y - 2)^2(\text{d}P/\text{d}x) = \text{const}$. For designing capillary range simulations, Section 5.6, we use a proportionality law to initialize body forces knowing results of just one simulation:

$$\begin{aligned} &\text{Ca}_{\text{lit}} \propto U_{\text{bubble}} \\ &U_{\text{bubble}} \propto \frac{\text{d}P}{\text{d}x} H_{\text{eff}}^2 \\ &\text{Ca}_{\text{lit}} \propto \frac{\text{d}P}{\text{d}x} H_{\text{eff}}^2 \quad \text{or} \\ &\frac{\text{d}P}{\text{d}x} \propto \frac{\text{Ca}_{\text{lit}}}{H_{\text{eff}}^2}, \end{aligned} \tag{10}$$

where the subscript "lit" stands for the predicted capillary number [10,3].

Table 1
The results for steady-state calculations. The simulated domain is of size 202×3000. U_{bubble} is the velocity of the interface at the fron tip of the bubble. Ca = 0.05 was taken to initialize the simulation. One can see that in terms of velocities and film thicknesses 100,000–300,000 iterations are enough.

N_{iter}	δ	U_{bubble}	Re
100,000	0.0655	0.0027	0.81
140,000	0.0608	0.0027	0.81
180,000	0.0577	0.0027	0.81
220,000	0.0630	0.0027	0.81
260,000	0.0660	0.0027	0.81
300,000	0.0661	0.0027	0.81

5.2. Steady state

The simulations were performed in order to determine the number of iterations for the bubble to reach the steady state. The grid was chosen as 202×3000. The body force was 0.375×10^{-6}. The initial film thickness was taken as 12 nodes. Table 1 summarizes the simulation results in terms of the film thickness in the middle of the bubble and the velocity of the interface as a function of time. We can conclude that it is enough to have 100,000–300,000 iterations for the bubble to approach the steady state.

5.3. Grid refinement

To properly estimate the interface resolution one needs to study the convergence as a function of the grid resolution. To do that the grid resolution is varied while all remaining parameters, including the bubble velocity and the capillary number, are fixed. Our goal is to determine the ratio of the interface thickness to the film thickness at which results are no longer dependent on the grid resolution.

Let us illustrate the procedure for the capillary number 0.05. The procedure of parameters choice and film thickness measurements follows the instructions from Section 5.1.

The simulations start from the initial grid size with $N_y = 102$, which gives the horizontal grid size as $N_x = 15(N_y - 2) = 1500$, and

Please cite this article in press as: A. Kuzmin, et al., Simulations of gravity-driven flow of binary liquids in microchannels, Chem. Eng. J. (2011), doi:10.1016/j.cej.2011.04.023

Table 2
The parameters and results for grid resolution. The simulated domain is of size $N_x \times N_y$. U_{bubble} is the velocity of the interface at the fron tip of the bubble. 5ξ is the interface thickness. $H_{\text{film}} = \delta(N_y - 2)$ is the size of the film in lattice Boltzmann units. Ca = 0.05 was taken to initialize the simulation.

N_x	N_y	δ	U_{bubble}	$\frac{5\xi}{H_{\text{film}}}$	N_{iter}	Re
1500	102	0.0694	0.0028	0.824	200,000	0.44
1875	127	0.0690	0.0028	0.646	250,000	0.53
2250	152	0.0675	0.0027	0.539	300,000	0.63
2625	177	0.0674	0.0027	0.453	350,000	0.73
3000	202	0.0662	0.0027	0.400	400,000	0.83
3375	227	0.0664	0.0026	0.355	450,000	0.91

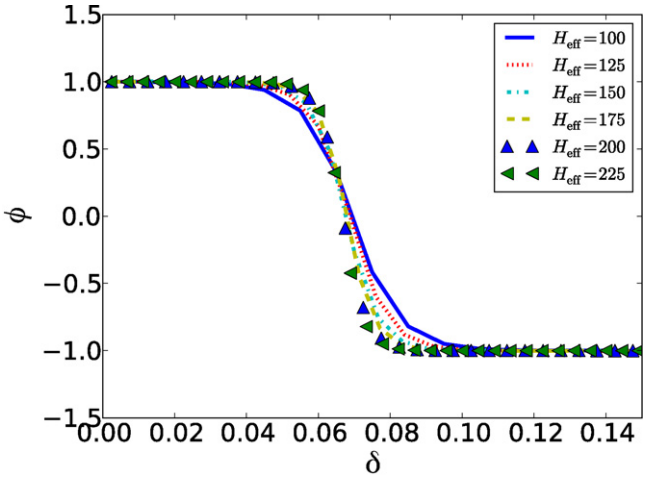

Fig. 4. Grid-refined profiles for the effective channel widths $H_{\text{eff}} = 100, 125, 150, 175, 200, 225$. δ is scaled on H_{eff} and $\delta = 0$ corresponds to the wall location. The profiles were taken at $x = 14$ (nondimensional coordinates). Capillary number is Ca = 0.05. The capillary number obtained from simulations Ca = 0.047.

proceeds with finer grids. The bubble is initialized as a rectangular box with coordinates $y = 7(N_y - 2)/100 \ldots N_y - 7(N_y - 2)/100 - 1$, $x = (N_x)/3 \ldots (2N_x)/3$ and phase $\phi_{\text{bubble}} = -1$. All other nodes are initialized with the phase field $\phi = 1$. The force gradient can be estimated through the Poiseuille profile formula, Eq. (6), and it equals 1.508×10^{-6} lattice units.

After choosing the reference parameters, the grid refinement procedure needs to keep the macroscopic parameters constant, see Section 5.1. We performed a number of simulations for the prescribed grids. The simulation results in terms of grid dimensions N_x, N_y, the film thickness δ, center bubble velocity U_{bubble} are summarized in Table 2. The unified scaled profiles are shown in Fig. 4. One can see that results converge for $H_{\text{eff}} \geq 175$, and that with proper initialization techniques, large enough time and different wall wettabilities, results are different only in the 3rd digit even for underresolved film thicknesses. To calculate how well the interface is resolved, the ratio of the interface thickness to the film thickness is calculated. The interface itself occupies approximately 5ξ, where $\xi = \sqrt{k/A} = 1$. The ratio of the interface thickness to the film thickness $5\xi/H_{\text{film}}$ is shown in Table 2. Based on these results one can conclude that the interface needs to be resolved as 40–50 percent of the expected film thickness for simulations to be grid independent. We further examine the velocities in the center of the bubble to calculate the capillary number. One can see from Table 2 that the bubble velocities are consistent and the calculated capillary number corresponding to these velocities is 0.047, which is close to the capillary number we aimed for. The corresponding difference can be attributed to the Poiseuille profile body force initialization.

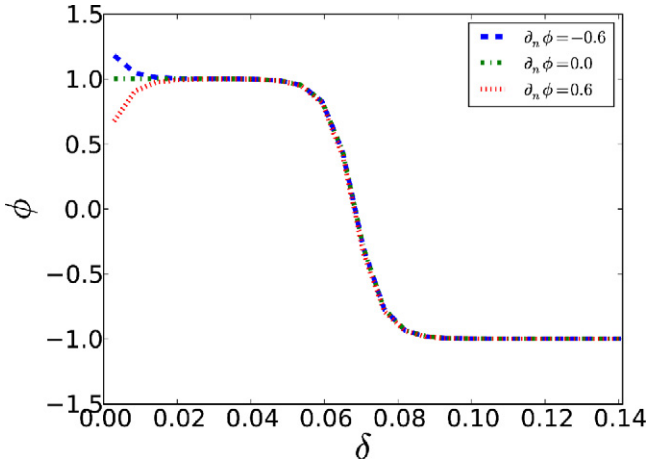

Fig. 5. Phase profiles for different wall gradients. One can see that if the thickness is properly resolved then the wettability of the wall does affect the film thickness. The simulations were conducted for 200,000 iterations. The measured profile was taken at the nondimensional coordinate scaled to H_{eff} as $x = 11.42$. Ca = 0.05 was taken to initialize simulation.

5.4. The influence of the wall gradient

The simulation results should not depend on the wall wettability. Wettability is defined through the phase gradient [22], $\partial_n\phi$. We took a large enough grid in order for simulations to be consistent – the grid size was 177×2626 and the initial film thickness was 12 lattice Boltzmann units, which corresponds to the predicted film thickness. We examined 11 different values for the wall gradient ranging from -1 to 1. The parameters and results are summarized in Table 3. The results are consistent for all the wall gradients given that the interface is properly resolved. For given wall gradients the values of interface thickness values are of 0.2% relative accuracy. For the given wall gradients 0.8 and 1.0 the simulations are unstable. One can see a few of the calculated phase profiles in Fig. 5. It shows that the negative wall gradient values cause non-physical phase values (above 1.0 near the wall). One should attribute them to the numerical adjustment of wall gradients through a first-order finite difference scheme. Note that negative values of the phase gradient are preferable, since the phase of the liquid adjacent to the wall has the value of 1. The phase values near the wall are above 1 and do not interact with the bubble which has phase value -1. In case of positive gradients, the values near the wall are below 1, and the gradient profile can merge with the values of the gas phase. Such a situation would correspond to slug flow when gas is in contact with the wall.

Another question that arises is the influence of the wall gradient on the bubble velocity and the corresponding capillary number. The shear stress controlled by the wall phase gradient changes the effective viscosity near the wall and the bubble velocity respec-

Table 3
The parameters and results for wall gradient effects on the film thickness. U_{bubble} stands for the interface velocity. δ is the film thickness. $\partial_n\phi$ is the phase gradient near the wall responsible for hydrophilic and hydrophobic behavior. The results are calculated at the middle of the bubble after 200 000 time iterations. Ca = 0.05 was taken to initialize the simulations.

$\partial_n\phi$	−1.0	−0.8	−0.6	−0.4	−0.2	0.0	0.2	0.4	0.6	0.8	1.0
δ	0.0633	0.0634	0.0634	0.0634	0.0634	0.0634	0.0633	0.0632	0.0631	N/A	N/A
U_{bubble}	0.0041	0.0042	0.0042	0.0042	0.0041	0.0041	0.0042	0.0042	0.0042	N/A	N/A

Please cite this article in press as: A. Kuzmin, et al., Simulations of gravity-driven flow of binary liquids in microchannels, Chem. Eng. J. (2011), doi:10.1016/j.cej.2011.04.023

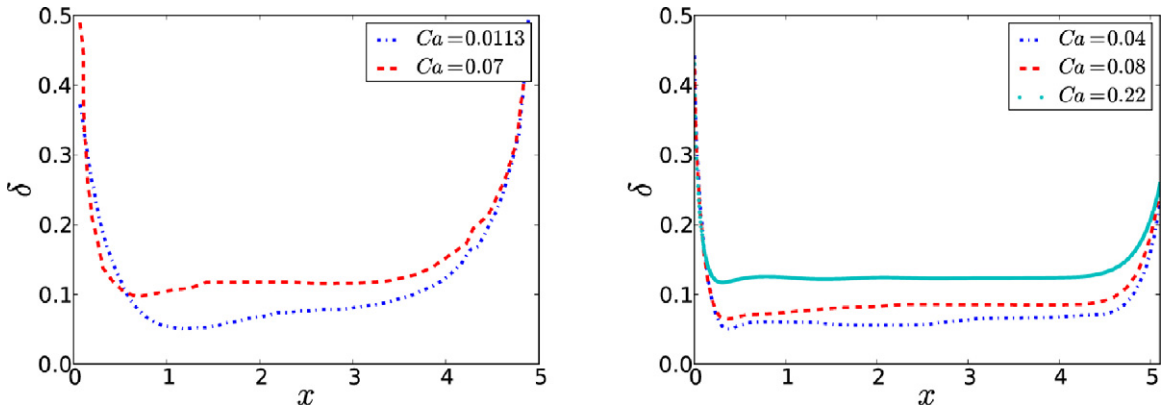

Fig. 6. A qualitative comparison for the film thickness across the bubble length. Left (courtesy of Yang et al. [16]), Right (present simulations); x is scaled to H_{eff} and increases in the flow direction. The data from [16] was digitally acquired by the program "Engauge Digitizer" and scaled to compare with the present simulations.

tively. If the viscosity ratio is high enough then the free surface motion of the bubble should not depend on the shear stress near the wall. One can see that if the film thickness is resolved properly the influence of the wall gradient can be neglected. The velocities of the bubble center for profiles along x direction are presented in Table 3. The average relative error for the mean velocity is 0.1%.

5.5. The film variation over the bubble

Next, we investigated the variation of the film thickness over the bubble length. The comparison for the thickness variation is presented in Fig. 6. One can see a qualitative agreement, i.e. the thickness increases towards the front meniscus and rapidly decreases towards the rear meniscus. This shape is sometimes referred as a "bullet" shape. The shape of the bubble is an important quantity, as the bubble tip shape mainly influences the film thickness at infinity [1]. It was indicated by Heil [3] that inertia effects influence insignificantly the film thickness at infinity but influence significantly the velocity pattern in front of the bubble. Therefore, to properly describe the Bretherton phenomena the bubble shape along with velocity pattern needs to be examined.

5.6. Capillary number region

The purpose of this section is to validate the correlations of Giavedoni and Saita [10] and Heil [3] for a range of capillary numbers. Because of limited computational resources, we skip the small capillary numbers and make calculations for the range of capillary numbers 0.03–0.8, which is a computationally reasonable task. To be consistent with the previous sections, we choose the grid to be 202×3001. Then 5 lattice Boltzmann units do not occupy more than 60 percent of the effective film thickness. Because the simulation gets unstable with smaller grids and larger gradients, all the capillary number simulations were performed on the same grid. To properly initialize the body force, the proportionality law was utilized. The forcing $6 \times 10^{-6}/16$ was chosen to obtain the predicted capillary number 0.05. The pressure gradient can be obtained through the capillary number ratio, see Section 5.1:

$$\frac{dP}{dx} = \frac{6 \times 10^{-6}}{16} \frac{\text{Ca}_{\text{lit}}}{0.05} \tag{11}$$

The film thickness is initialized through the ratio of capillary numbers as well:

$$12 \frac{\text{Ca}_{\text{lit}}}{0.05}$$

The results obtained after 2×10^5 steps are presented in Table 4. We chose to measure the film thickness in the middle of the bubble.

Table 4
The parameters and results for capillary number region simulations. δ_{lit} is the film thickness with corresponding Ca_{lit} taken from literature. δ is the simulation film thickness with corresponding Ca.U_{bubble} is the interface velocity at the center axis. Ca is based on the measured bubble tip velocity U_{bubble}.

Ca_{lit}	δ_{lit}	δ	U_{bubble}	Ca	Re
0.03	0.04	0.040	0.0014	0.026	0.449
0.05	0.06	0.058	0.0027	0.047	0.820
0.08	0.08	0.085	0.0045	0.080	1.378
0.1	0.1	0.076	0.0037	0.065	1.126
0.2	0.12	0.122	0.0125	0.222	3.807
0.4	0.13	0.151	0.0271	0.479	8.222
0.6	0.15	0.164	0.0416	0.736	12.617
0.8	0.16	0.172	0.0559	0.989	16.960

The classical Bretherton formulation is for the measurement of the film thickness at "infinity". However, Thulasidas et al. [28] indicate that for the gravity-driven bubble train flow in tubes it is enough for bubbles to have a length of two–three tube diameters to apply analysis for very long bubbles. In comparison with the axisymmetric geometry, for three-dimensional square shaped microchannels Hazel and Heil [29] indicate the measurement of the film thickness at 5.5 channel heights from the front bubble tip. This distance was shown sufficient for the film thickness to establish itself for the capillary number range $\text{Ca} < 4$. Giavedoni and Saita [10] showed that the film stabilizes at the distances of 2.6–4.0 diameters from the front tip depending on the Reynolds number. We chose to measure the film thickness in the middle of the bubble, which is located at least at a distance of 2.5–3 channel heights from the bubble tip. Moreover, the film thickness examination, see Section 5.5, shows that for the capillary range of interest, i.e. $0.05 \leq \text{Ca} \leq 1$, the standard deviation of the film thickness from the bubble middle film thickness is around 7 percent for small capillary numbers ($\text{Ca} = 0.05$) and less than 1 percent for larger ones ($\text{Ca} \geq 0.1$). This certainly validates the point of choice to measure bubble thickness. One can see that the calculated capillary numbers are overpredicted but the obtained thicknesses are overpredicted as well due to the body force setting caused by the Poiseuille flow assumption. If one needs to obtain the desired capillary number, the shooting method for the forcing is necessary, starting with the Poiseuille pressure gradient force as the initial condition. Note that in the present work the shooting method is not used but it is presented as a possible remedy to exactly match the required capillary number. We extracted the data of Giavedoni and Saita [10] and Heil [3] and compared them with our results (see Fig. 7).

For the completeness of the presented data we also indicate the velocity streamlines profiles, Fig. 8. The pattern shows that there is a transition of having vortex in the front of the bubble for $\text{Ca} = 0.22$

Please cite this article in press as: A. Kuzmin, et al., Simulations of gravity-driven flow of binary liquids in microchannels, Chem. Eng. J. (2011), doi:10.1016/j.cej.2011.04.023

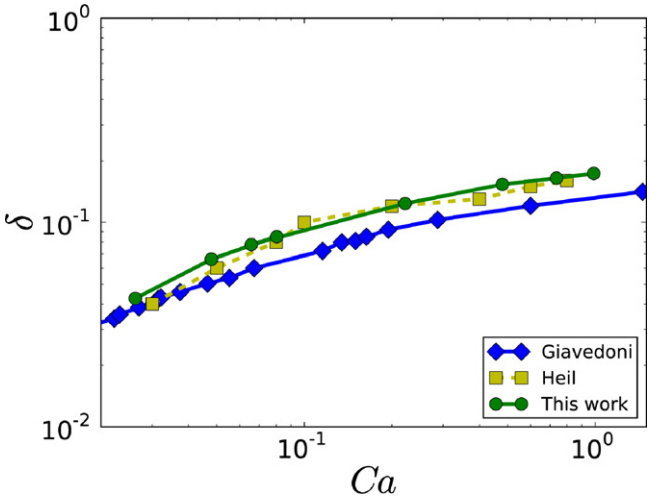

Fig. 7. A comparison between simulation results and results of Giavedoni and Saita [10] and Heil [3]. One can see a reasonable agreement. The plots depict the film thickness as a function of the the capillary number. Data from [10] was extracted with the help of "Engauge Digitizer", data from Heil [3] was extracted manuallys using a set of curves involving interpolation and is the reason while the data exhibits a noisy trend.

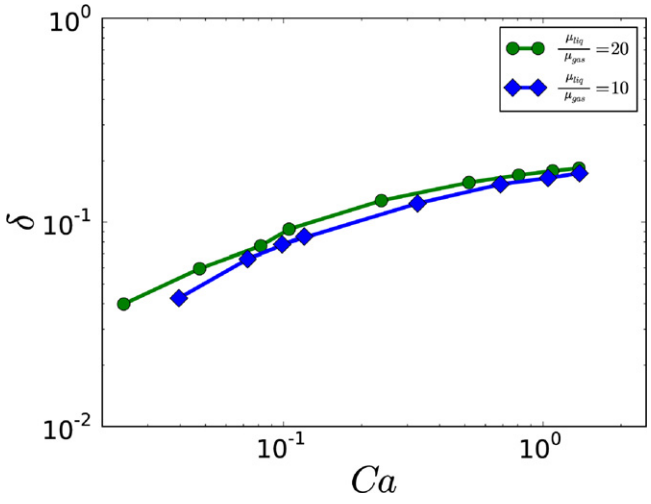

Fig. 9. The film thicknesses versus capillary number for $\mu_{liq}/\mu_{gas} = 10$ and $\mu_{liq}/\mu_{gas} = 20$.

and not having it for larger capillary numbers Ca = 1.00. Giavedoni and Saita [10] studied the behavior of the detaching of the vortex for the Bretherton problem. They indicate critical capillary numbers as Ca = 0.73 and Ca = 0.89 for detaching and full vortex disappearance. Heil [3] indicates that the behavior of the pattern strongly depends on the Reynolds number. The scope of this work is to indicate the qualitative capture of the effects.

5.7. The influence of different viscosities ratio

The results presented above are taken for the liquid over gas kinematic viscosity ratio of 10. We performed the same simulations for the liquid over gas viscosity ratio of 20. The relaxation parameters were taken as $\tau_{liquid} = 4.5$ and $\tau_{bubble} = 0.7$. We did not find any significant differences from the results presented above. The comparison for the liquid film thicknesses is presented in Fig. 9. The results validate our assumption that in the low capillary flow regime the sufficiently high gas over liquid viscosity ratio ($\geq$10) is sufficient to obtain results consistent with the literature data. However, in reality the viscosity ratio affects results as it is indicated by Han and Shikazono [30].

Also, while it is necessary to increase the viscosities ratio for the binary-liquid formulation to be close to the physical Bretherton formulation, one needs to be attentive to the numerical accuracy of the LBM formulation. It is known [31] that the BGK collision operator used in the present scheme has residual error accuracy proportional to $(\tau - 1/2)^2$. That means that by increasing the viscosity one

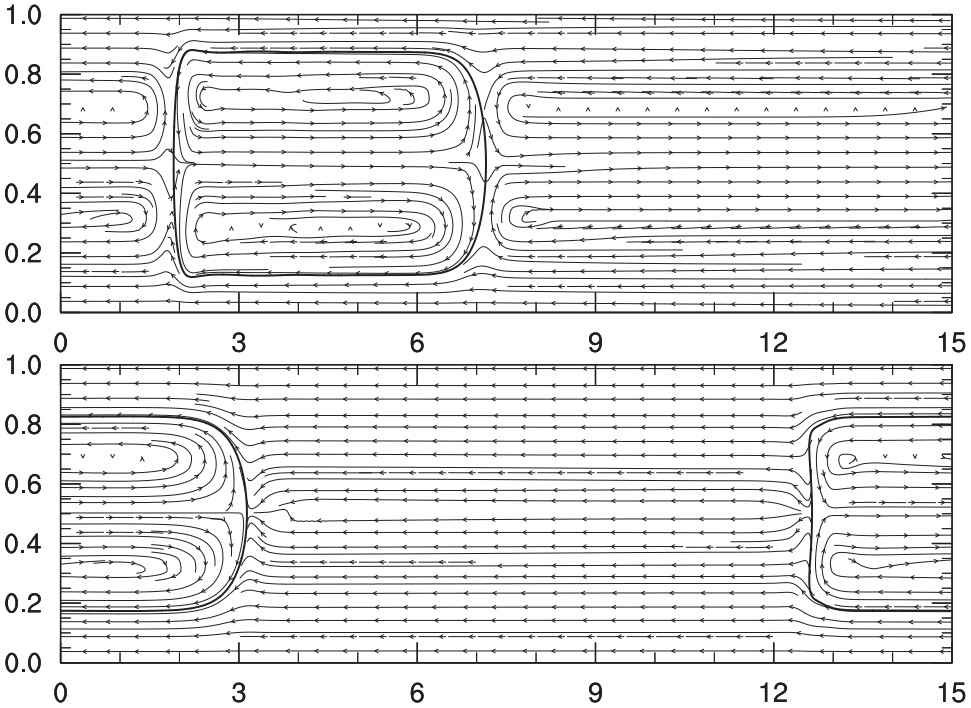

Fig. 8. The streamlines plots for Ca = 0.22 (top) and Ca = 1.00 (bottom). One can see the change of pattern as indicated in works of Heil [3] and Giavedoni and Saita [10]. For smaller capillary numbers there exists a vortex in front of the bubble. For the larger once there is none. The streamlines are presented in the reference frame moving with the bubble interface.

Please cite this article in press as: A. Kuzmin, et al., Simulations of gravity-driven flow of binary liquids in microchannels, Chem. Eng. J. (2011), doi:10.1016/j.cej.2011.04.023

reduces the spatial accuracy of the method. To avoid this one needs to use advanced formulations of the LBM collision operator, such as two-relaxation-times (TRT) and multiple-relaxation-times (MRT) collision operators [32]. Although TRT and MRT collisions operators are studied for simple hydrodynamics solutions, their application to complex fluid flows is sparse and not studied well.

6. Conclusion

This work presents numerical studies of the Bretherton/Taylor problem using the binary liquid lattice Boltzmann method. The bubble was chosen sufficiently long for the film thickness to stabilize, and periodic boundary conditions were used to keep the simulations robust. A bubble train was simulated instead of the motion of a single bubble, and care was taken to minimize the mutual influence of neighboring bubbles. The computational results in terms of capillary number dependence and shape of the bubbles show consistency with the previously published data. Surprisingly, with large enough viscosity ratio the results are independent of any inertial effects. An examination of the influence of grid resolution on the results allowed us to determine that the phase interface should be resolved as at least 50 percent of the film thickness in order for the simulations to be grid independent. Though our results are specific to the binary liquid lattice Boltzmann method, the numerical hints and procedures can be used for any continuous interface method.

Acknowledgements

A. Kuzmin wants to thank Schlumberger for financial support. Authors are grateful to referees for their significant contribution to the quality improvement of the manuscript.

References

[1] F. Bretherton, The motion of long bubbles in tubes, J. Fluid Mech. 10 (1960) 166–188.
[2] D. Ingham, J. Ritchie, The motion of a semi-infinite bubble between parallel plates, Z. Math. Phys. 43 (1992) 191–206.
[3] M. Heil, Finite Reynolds number effects in the Bretherton problem, Phys. Fluids 13 (2001) 2517–2521.
[4] D. Yu, R. Mei, L.-S. Luo, W. Shyy, Viscous flow computations with the method of lattice Boltzmann equation, Prog. Aerospace Sci. 39 (2003) 329–367.
[5] S. Ansumali, I. Karlin, H. Öttinger, Minimal entropic kinetic models for hydrodynamics, Europhys. Lett. 63lu (2003) 798–804.
[6] S. Ansumali, I. Karlin, C. Frouzakis, K. Boulouchos, Entropic lattice Boltzmann method for microflows, Physica A 359 (2006) 289–305.
[7] G. Falcucci, G. Chiatti, S. Succi, A. Mohamad, A. Kuzmin, Rupture of a ferrofluid droplet in external magnetic fields using a single-component lattice Boltzmann model for nonideal fluids, Phys. Rev. E 79 (2009) 1–5.
[8] M. Swift, W. Osborn, J. Yeomans, Lattice Boltzmann simulation of nonideal fluids, Phys. Rev. Lett. 75 (1995) 831–834.
[9] X. Shan, H. Chen, Simulation of nonideal gases and gas–liquid phase transitions by the lattice Boltzmann equation, Phys. Rev. E 49 (1994) 2941–2948.
[10] M. Giavedoni, F. Saita, The axisymmetric and plane cases of a gas phase steadily displacing a Newtonian liquid – a simultaneous solution of the governing equations, Phys. Fluids 9 (1997) 2420–2428.
[11] H. Wong, C. Radke, S. Morris, The motion of long bubble in polygonal capillaries. Part 1. Thin films, J. Fluid Mech. 292 (1995) 71–94.
[12] H. Wong, C. Radke, S. Morris, The motion of long bubbles in polygonal capillaries. Part 2. Drag, fluid pressure and fluid flow, J. Fluid Mech. 292 (1995) 95–110.
[13] M. Kreutzer, M. van der Eijnded, F. Kapteijn, J. Moulijn, J. Heiszwolf, The pressure drop experiment to determine slug lengths in mulitphase monoliths, Catal. Today 105 (2005) 667–672.
[14] J. van Baten, R. Krishna, CFD simulations of mass transfer from Taylor bubbles rising in circular capillaries, Chem. Eng. Sci. 59 (2004) 2535–2545.
[15] R. Ledesma-Aguilar, I. Pagonabarraga, A. Hernàndez-Machado, Three-dimensional aspects of fluid flows in channels. II. Effects of meniscus and thin film regimes on viscous fingers, Phys. Fluids 19 (2007) 1–8.
[16] Z. Yang, B. Palm, B. Sehgal, Numerical simulation of bubbly two-phase flow in a narrow channel, Int. J. Heat Mass Transfer 45 (2002) 631–639.
[17] K. Fukagata, N. Kasagi, P. Ua-arayaporn, T. Himeno, Numerical simulation of gas–liquid two-phase flow and convective heat transfer in a micro tube, Int. J. Heat Fluid Flow 28 (2007) 72–82.
[18] D. Lakehal, G. Larrignon, C. Narayanan, Computational heat transfer and two-phase flow topology in miniature tubes, Microfluidics Nanofluidics 4 (2008) 261–271.
[19] A. Carlson, P. Kudinov, C. Narayanan, Prediction of two-phase flow in small tubes: a systematic comparison of state-of-the-art cmfd codes, in: 5th European Thermal-Sciences Conference, The Netherlands, 2008.
[20] Z. Guo, C. Zheng, B. Shi, Discrete lattice effects on the forcing term in the lattice Boltzmann method, Phys. Rev. E 65 (2002) 1–6.
[21] L. Landau, E. Lifshitz, Fluid Mechanics, Pergamon, Oxford, 1987.
[22] C. Pooley, H. Kusumaatmaja, J. Yeomans, Contact line dynamics in binary lattice Boltzmann simulations, Phys. Rev. E 78 (2008) 1–9.
[23] R. Ledesma-Aguilar, A. Hernàndez-Machado, I. Pagonabarraga, Three-dimensional aspects of fluid flows in channels. I. Meniscus and thin film regimes, Phys. Fluids 19 (2007) 1–10.
[24] B. Noye, R. Arnold, Accurate finite difference approximations for the Neumann condition on a curved boundary, Appl. Math. Model. 14 (1990) 1–12.
[25] B. Hunt, Finite difference approximation of boundary conditions along irregular boundaries, Int. J. Numer. Meth. Eng. 12 (1978) 229–235.
[26] I. Halliday, L. Hammond, C. Care, K. Good, A. Stevens, Lattice Boltzmann equation hydrodynamics, Phys. Rev. E 64 (2001) 1–8.
[27] I. Ginzburg, D. d'Humières, Multireflection boundary conditions for lattice Boltzmann models, Phys. Rev. E 68 (2003) 1–30.
[28] T. Thulasidas, M. Abraham, R. Cerro, Bubble-train flow in capillaries of circular and square cross section, Chem. Eng. Sci. 50 (1995) 183–199.
[29] A. Hazel, M. Heil, The steady propagation of a semi-infinite bubble into a tube of elliptical or rectangular cross-section, J. Fluid Mech. 470 (2002) 91–114.
[30] Y. Han, N. Shikazono, Measurement of liquid film thickness in micro square channel, Int. J. Multiphase Flow 35 (2009) 896–903.
[31] I. Ginzburg, F. Verhaeghe, D. d'Humières, Study of simple hydrodynamic solutions with the two-relaxation-times lattice Bolzmann scheme, Commun. Comput. Phys. 3 (2008) 519–581.
[32] I. Ginzburg, Equilibrium-type and link-type lattice Boltzmann models for generic advection and anisotropic-dispersion equation, Adv. Wat. Res. 28 (2005) 1171–1195.

Please cite this article in press as: A. Kuzmin, et al., Simulations of gravity-driven flow of binary liquids in microchannels, Chem. Eng. J. (2011), doi:10.1016/j.cej.2011.04.023